Chemical Physics 539 (2020) 110961

Contents lists available at ScienceDirect

Chemical Physics

journal homepage: www.elsevier.com/locate/chemphys

The effect of autoionization on the HBr^+ X $^2\Pi_{3/2,1/2}$ state photoelectron angular distributions

H.R. Hrodmarsson[a], B. Gans[b], S. Boyé-Péronne[b], G.A. Garcia[a], L. Nahon[a], S.T. Pratt[c], D.M.P. Holland[d,*]

[a] Synchrotron SOLEIL, L'Orme des Merisiers, Saint-Aubin, BP 48, 91192 Gif-sur-Yvette, France
[b] Institut des Sciences Moléculaires d'Orsay, CNRS, Université Paris-Saclay, F-91405, France
[c] Chemical Sciences and Engineering Division, Argonne National Laboratory, Lemont, IL 60439, USA
[d] Daresbury Laboratory, Daresbury, Warrington, Cheshire WA4 4AD, UK

ARTICLE INFO

Keywords:
Hydrogen bromide
Photoelectron angular distributions
Autoionizing Rydberg states
Threshold photoelectron spectrum

ABSTRACT

A double-imaging photoelectron-photoion spectrometer and synchrotron radiation have been used to measure the HBr^+ X $^2\Pi_{3/2}$ $v^+ = 0$, 1, 2 and the $^2\Pi_{1/2}$ $v^+ = 0$ state photoelectron angular distributions, as characterized by the anisotropy parameter β, the total ion yield, and the threshold photoelectron spectrum. Particular attention has been focussed on the photon energy range between the $^2\Pi_{3/2}$ and the $^2\Pi_{1/2}$ spin–orbit components of the ground ionic state. This region encompasses Rydberg states, belonging to series converging onto the upper $^2\Pi_{1/2}$ ionization limit, which may decay by autoionization into the $^2\Pi_{3/2}$ ionization continuum. A detailed study has been performed on the effects of autoionization on the $^2\Pi_{3/2}$ $v^+ = 0$ state photoelectron angular distributions. The observed energy dependent variations in the β-values exhibit a regular pattern that correlates with excitation into members of a very broad d-type Rydberg series. Additional rapid variations in the β-parameters, which occur over a narrow energy range, appear to coincide with sharp autoionizing Rydberg states belonging to s, p and d series. The present experimental results for the HBr^+ X $^2\Pi_{3/2}$ $v^+ = 0$ state photoelectron anisotropy parameter are compared to previously reported theoretical predictions and to earlier studies of the Kr^+ $4p^5$ $^2P_{3/2}$ state β-parameter. The threshold photoelectron spectrum of the X $^2\Pi_{3/2}$ $v^+ = 0$ band exhibits partially resolved rotational structure. A simulation of this structure yields an ionization threshold of 11.6673 ± 0.0010 eV, which is consistent with previous measurements.

1. Introduction

Experimental and theoretical studies of the Rydberg states formed through excitation of the outermost p-orbital in the rare gases have played an important role in developing our understanding of the spectroscopy and dynamics of photon absorption in gas phase systems (see Sukhorukov et al. [1] for a recent review). Of particular interest has been the energy region lying between the ground $^2P_{3/2}$ and excited $^2P_{1/2}$ spin–orbit split ionic states associated with this orbital. Taking krypton as an example, electric dipole selection rules allow transitions from the $4p^6$ $^1S_0$ ground state into two Rydberg series, $4p^5(^2P_{1/2})ns[1/2]_1$, and $4p^5(^2P_{1/2})nd[3/2]_1$, converging onto the $^2P_{1/2}$ ionization limit. Rydberg states belonging to these series may decay (autoionize) into the $^2P_{3/2}$ + e^- continuum, with the *n*s and *n*d states resulting, respectively, in sharp and broad resonances in the ion yield [2]. Autoionization affects not only the photoabsorption and photoionization spectra but also the photoionization dynamics, as characterized by the anisotropy parameter, β, describing the photoelectron angular distribution. For Kr, calculations performed by Dill [3] show that the β-parameter exhibits pronounced variations with energy across regions containing autoionizing resonances. These predictions have been confirmed experimentally [4–6] for the $4p^6(^1S_0) \rightarrow 4p^5(^2P_{1/2})$ *n*s and *n*d Rydberg series in krypton.

Hydrogen bromide is isoelectronic with krypton and has a valence shell electronic configuration of $(4s\sigma)^2(4p\sigma)^2(4p\pi)^4$ $^1\Sigma^+$. The outermost $4p\pi$ orbital is non-bonding, and corresponds closely to an atomic bromine 4p orbital oriented perpendicular to the molecular axis. Photoionization of the $4p\pi$ orbital gives rise to the HBr^+ X $^2\Pi_{3/2}$ and $^2\Pi_{1/2}$ spin–orbit components, and leads to only a small change in the equilibrium bond length. Consequently, the X state photoelectron, and threshold photoelectron, spectra [7–12] are dominated by peaks due to the $^2\Pi_{3/2,1/2}$ $v^+ = 0$ states, with only weak accompanying structure

* Corresponding author.
E-mail address: david.holland@stfc.ac.uk (D.M.P. Holland).

https://doi.org/10.1016/j.chemphys.2020.110961
Received 10 June 2020; Received in revised form 5 August 2020; Accepted 18 August 2020
Available online 20 August 2020

associated with vibrationally excited levels. The photoionization spectrum of HBr, in the energy range (~11.6–12.0 eV) between the $^2\Pi_{3/2}$ and $^2\Pi_{1/2}$ ionization limits, has been measured using radiation from a helium continuum light source [13], and by employing a laser-based light source where the VUV radiation is generated by nonlinear frequency mixing [14]. Assignments for the structure observed in the ion yield have been proposed through consideration of the measured quantum defects [14], and by comparison with theoretical predictions obtained using multichannel quantum defect theory [13,15]. As in the spectrum of Kr, the *n*s and *n*d Rydberg series of HBr converging onto the upper $^2\Pi_{1/2}$ spin–orbit component are strongest, but the non-spherical nature of the molecule also leads to the observation of *n*p and *n*f series [13–15].

The lowest ionization threshold of the X $^2\Pi_{3/2}$ $v^+ = 0$ state has been determined to be 11.6667 ± 0.0001 eV from single photon electron yield measurements [14], and 11.6668 ± 0.0001 [16] and 11.6669 ± 0.0002 [17] eV from zero-kinetic-energy pulsed-field-ionization (ZEKE-PFI) experiments. Ionization energies of the ground and vibrationally excited levels of the X $^2\Pi_{3/2,1/2}$ states have been reported by Yencha et al. [12].

The valence shell photoionization dynamics have been studied over an extended photon energy range through measurements of the photoionization partial cross sections, photoelectron angular distributions and spin polarization parameters [18–21]. These experimental results have been compared to the corresponding theoretical predictions [19,22]. A more detailed investigation has been performed in the energy region between the $^2\Pi_{3/2}$ and $^2\Pi_{1/2}$ ionization limits by measuring the spin polarization parameter, *A*, and comparing the experimental data with calculated values [15].

The theoretical work carried out by Irrgang et al. [15] also enabled the photoelectron anisotropy parameters β to be evaluated. The calculations predicted that autoionization from Rydberg states belonging to series converging onto the $^2\Pi_{1/2}$ ionization limit induces energy dependent variations in the β-values. The aim of the present experiment is to test these theoretical predictions. To this end, we have employed a double-imaging photoelectron-photoion spectrometer [23,24] and synchrotron radiation [25] to measure the total ion yield, the threshold photoelectron spectrum (TPES), and photoelectron energy dependent angular distributions in the photon excitation range 11.67–12.31 eV. The experimental results for the X $^2\Pi_{3/2}$ state β-parameter are compared to the corresponding theoretical predictions [15]. They are also discussed in relation to the analogous experimental [4–6] and theoretical [26] results for the Kr^+ $4p^5$ $^2P_{3/2}$ state.

2. Experimental apparatus and procedure

The experiment was performed using synchrotron radiation emitted by DESIRS, a VUV undulator-based beamline at the SOLEIL electron storage ring, and a double-imaging photoelectron-photoion spectrometer. Detailed descriptions of the beamline [25], the gas filter used to suppress the undulator high harmonics [27], and the particle spectrometer, DELICIOUS III [23,24], have been reported previously.

Radiation from a variable polarization undulator, after passing through the gas filter, was focussed onto the monochromator entrance slit. For the present work, the entrance and exit slit widths were set at 40 μm, which, when combined with the 2400 grooves/mm grating, gave a resolution of 0.3 meV (FWHM) at a photon energy of 12 eV. The gas filter, containing argon, suppressed any contributions from the undulator higher harmonics over the photon energy range relevant to the present experiment. The undulator was adjusted to provide 100% plane polarized radiation within the electron detection plane of the Velocity Map Imaging (VMI) spectrometer [28] part of DELICIOUS III. The photoelectron angular distributions were determined relative to the polarization axis.

HBr gas (Sigma Aldrich, with a stated impurity ≥ 99%) entered the spectrometer in the form of an unseeded molecular beam. No carrier gas was used. The sample gas, at a backing pressure of 0.4–0.6 bar, was expanded through a 30 μm nozzle and traversed two skimmers, each having a 2 mm diameter, before being ionized with synchrotron radiation in the centre of DELICIOUS III. The translational temperature of the beam was estimated as ~ 60 K, using the procedure described by Holland et al. [29]. If it is assumed that the rotational temperature of the HBr molecules is similar to the translational temperature, then the maximum of the ground state rotational population occurs in $J = 1$, and ~ 96% of the sample is in levels with $J \leq 3$. As discussed below, the rotational temperature of ~ 60 K is consistent with our modelling of the TPES.

Photoelectron images of the HBr^+ X $^2\Pi_{3/2,1/2}$ states were recorded with the double-imaging spectrometer operating in coincidence mode. This mode of operation facilitates the subtraction of any electron signal not originating from the parent molecule (for example, a background gas). Moreover, ionization processes originating from the cooled part of the molecular beam could be selected. The spatial response of the detector was taken into account by normalizing the photoelectron images by a 2D detection function recorded with photoelectrons from Xe having a large $\rho = KE/V_{rep} = 0.16$ ratio, *KE* being the electron energy and V_{rep} the repeller voltage of the VMI device. Under these conditions, ray-tracing simulations show that the curvature of the photoelectron Newton sphere is negligible, so that an ideal detector would record a perfectly homogenous image. Note that any angular anisotropies from photoionization of Xe are removed by using linearly polarized radiation with the polarization axis normal to the detector. Inversion and reconstruction of the detector response corrected images, to recover the central slice of the original three-dimensional distribution, were accomplished using the pBASEX software [30]. The inverted image was subsequently fitted to Eq.(1) (see below) to evaluate the photoelectron anisotropy parameters.

Some examples of mass-selected photoelectron velocity map images, recorded at photon energies of 11.766, 11.774 and 11.993 eV, are shown in Fig. 1. The image recorded at 11.774 eV illustrates the effect of autoionization on the photoelectron angular distributions. The left part of the images corresponds to the raw, untreated data, while the right shows the result of the Abel transformation using the pBasex algorithm.

For ionization of randomly oriented molecules by 100% plane polarized radiation, with electron detection in a plane perpendicular to the photon propagation direction, the photoionization differential cross section in the electric dipole approximation can be expressed as [31]:

$$\frac{d\sigma}{d\Omega} = \frac{\sigma}{4\pi}[1 + \beta P_2(\cos\theta)] \quad (1)$$

where σ is the angle-integrated partial cross section, $d\Omega$ is the differential solid angle element in the direction specified by the polar angle θ (electron ejection angle relative to the plane of polarization), and $P_2(\cos\theta)$ is the Legendre polynomial of second order.

The average anisotropy parameter, β_{av}, for a particular photoelectron band has been obtained after fitting a Gaussian function to the photoelectron spectrum as the weighted mean value across the half width at half maximum (HWHM) of the peak:

$$\beta_{av} = \frac{\sum_{-HWHM}^{+HWHM} \beta(KE)\sigma(KE)}{\sum_{-HWHM}^{+HWHM} \sigma(KE)} \quad (2)$$

The error bar takes into account the dispersion of the anisotropy parameter across the band:

$$\beta_{av}^{std} = \sqrt{\frac{m \sum_{-HWHM}^{+HWHM} \sigma(KE)[\beta(KE) - \beta_{av}]^2}{(m-1)\sum_{-HWHM}^{+HWHM} \sigma(KE)}} \quad (3)$$

where *m* is the number of non-zero $\sigma(KE)$ points.

The coincidence spectra also allow the extraction of a total ion yield and a TPES, the latter using a previously described method [32]. An

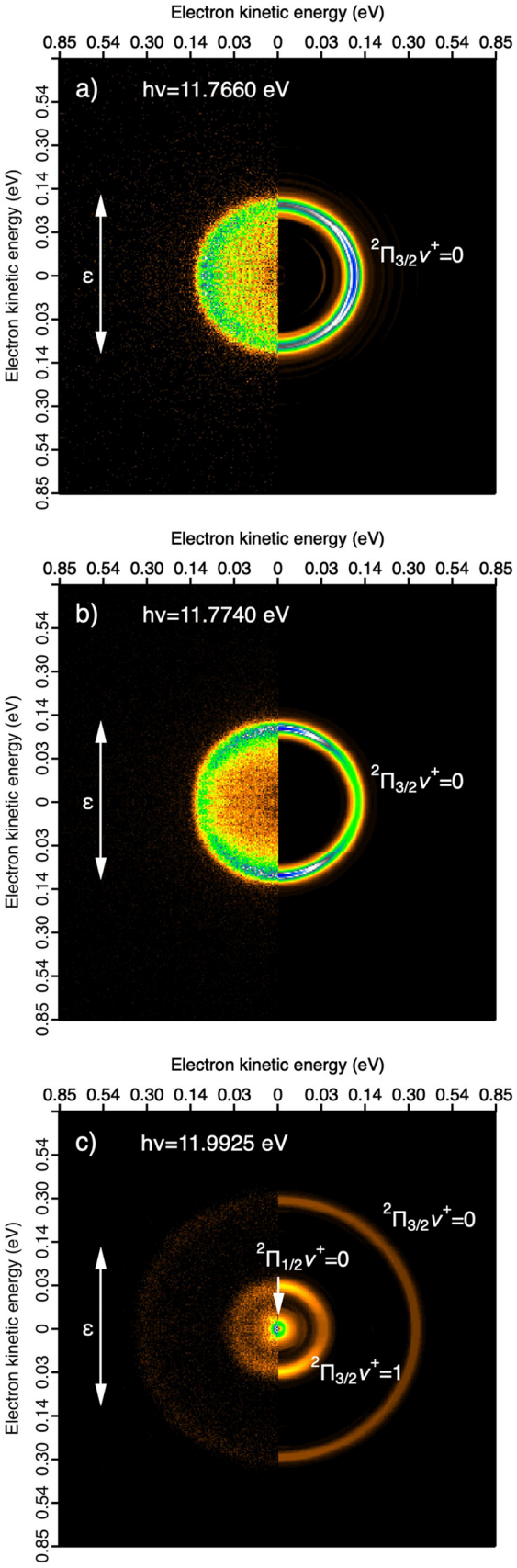

Fig. 1. Mass-selected photoelectron velocity map images of HBr recorded at photon energies of 11.766 eV (a), 11.774 eV (b) and 11.993 eV (c). The left part of the images corresponds to the raw, untreated data, while the right shows the result of the Abel transformation using the pBasex algorithm. The light is plane polarized in the vertical direction, as shown by the double-headed arrow. Since none of the spectra displayed any measurable differences between the $H^{79}Br$ and $H^{81}Br$ isotopologues, the data presented throughout this article result from the sum of both ion mass signals.

acquisition time of many hours was required to record electron images across the entire photon excitation range and the gas pressure was not completely stable over this extended period. Therefore, a fast scan with larger energy increments was recorded over the same energy range, and used to correct the overall shape of the longer scan. The variation in the incident photon intensity across the spectrum was monitored with a Si AXUV100 photodiode, whose efficiency was known. The photon energy scale was calibrated using the Ar 3p → 4s absorption line at 11.828 eV [33]. A sharp dip associated with this transition appears in the ion yield due to the use of argon in the high harmonic filter. In estimating the accuracy of the photon energy scale, we make use of this established transition energy, together with the excitation energies of the structure due to the autoionizing Rydberg states in HBr obtained in the high resolution ion yield measurements [14]. Further verification of the calibration is provided through comparison of the HBr^+ X $^2\Pi_{3/2}$ $v^+ = 0$ ionization energy determined in the present work with those reported previously [14,16,17]. This assessment leads to an absolute energy scale accuracy of 0.8 meV.

The experimental results reported in this article were collected during two beamtime allocations. In the first, spectra were measured over a photon energy range of 11.67–12.31 eV. This allowed the $v^+ = 0$, 1 and 2 levels of the $^2\Pi_{3/2}$ state, and the $v^+ = 0$ level of the $^2\Pi_{1/2}$ state to be studied. Fig. 2 shows photoelectron spectra extracted from the images recorded at photon energies of 12.0, 12.2 and 12.3 eV. These energies have been selected to display the evolution of the photoelectron spectrum near to the ionization thresholds of the higher vibrational levels. A total ion yield was recorded over the same photon energy range and a TPES was obtained over a slightly wider energy range.

The relative intensities of the vibrationally resolved photoelectron peaks shown in Fig. 2 differ somewhat from those observed at high photon energies, for example, in HeI excited photoelectron spectra [7–11], where direct ionization dominates. These differences may be due to low, energy dependent photoionization partial cross sections close to threshold and/or to the influence of autoionization from the numerous Rydberg states belonging to series converging onto vibrationally excited levels of the X $^2\Pi_{3/2,1/2}$ ionization thresholds. It is also conceivable that a poorer performance of the detector close to the centre may affect the relative intensities.

In the second allocation period, a more detailed investigation of the $^2\Pi_{3/2}$ $v^+ = 0$ state was performed over a smaller energy range (11.67–11.92 eV), enabling improved quality measurements of the $^2\Pi_{3/2}$ $v^+ = 0$ β-parameter to be obtained. Although the β-values derived in the second run were of superior quality in terms of experimental uncertainty, it should be emphasized that the energy dependent variations in the β-values over the two runs were similar, thereby providing a high degree of confidence in the observed structure.

In the second beamtime allocation, no indication was found for the presence of HBr clusters in the ion time-of-flight spectrum. However, in the first allocation, the ion time-of-flight spectrum (Fig. 3) revealed a weak dimer signal together with a discernible broad pedestal, centred around the monomer peak, attributed to dissociative ionization from clusters. In obtaining the data plotted in Figs. 1, 4 and 5, only the sharp parent peaks at 80 and 82 amu were taken into account. Under these conditions, we estimate that the contribution from dissociative ionization during the first beamtime allocation was less than 5%.

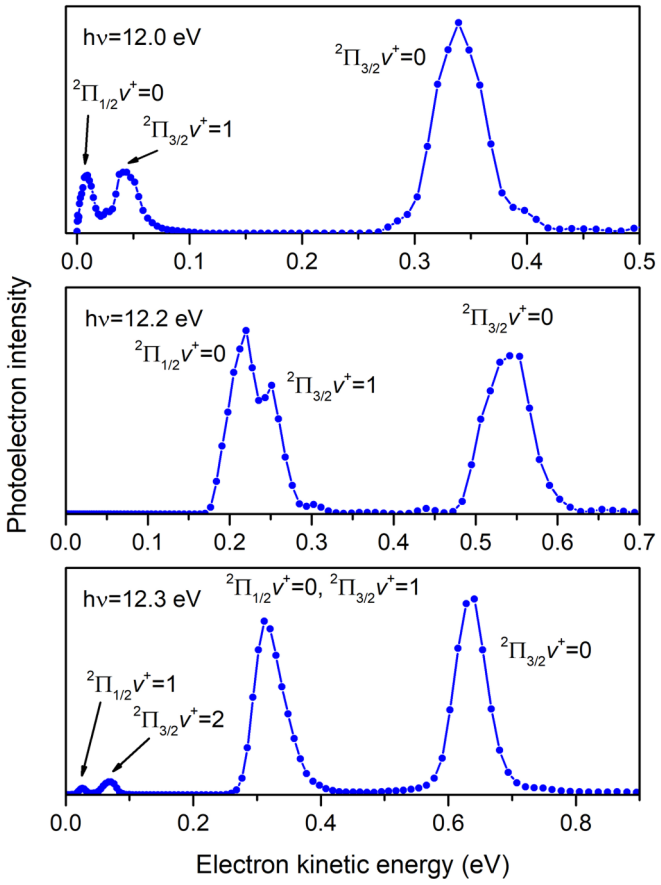

Fig. 2. Photoelectron spectra of the HBr^+ X $^2\Pi_{3/2}$ v^+ and the $^2\Pi_{1/2}$ v^+ states recorded at the photon energy given in each panel.

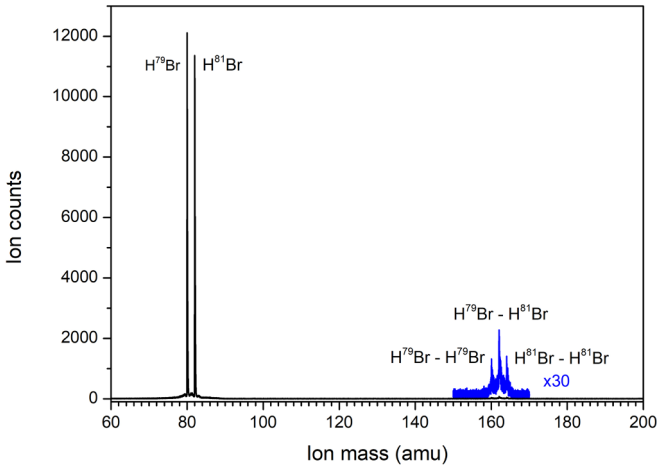

Fig. 3. Ion time-of-flight spectrum of HBr, integrated over the photon energy range 11.67 – 12.31 eV, recorded in the first beamtime allocation. The expanded section displays a weak dimer signal. A broad pedestal, centred around the monomer peak, is attributed to dissociative ionization from clusters.

3. Results and discussion

3.1. Overview of the valence shell photoelectron spectrum

Fig. 4(a) displays the experimental TPES in the region between the $^2\Pi_{3/2}$ v^+ = 0 and $^2\Pi_{1/2}$ v^+ = 0 ionization thresholds, as well as a simulation of the X $^2\Pi_{3/2}$ v^+ = 0 ← X $^1\Sigma^+$ and the X $^2\Pi_{1/2}$ v^+ = 0 ← X $^1\Sigma^+$ photoionizing transitions. Fig. 4(b) shows an expanded version of

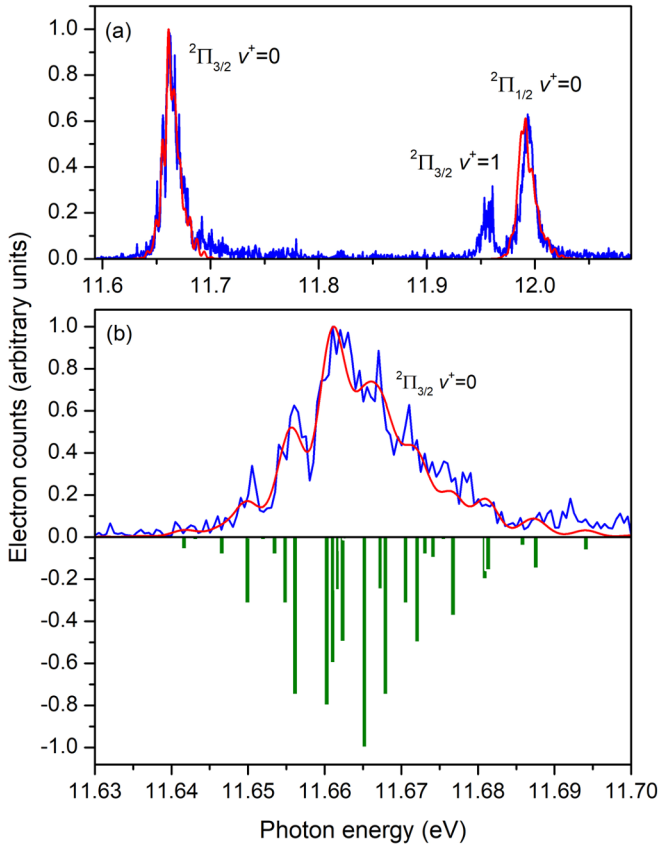

Fig. 4. (a) The threshold photoelectron spectrum (blue) in the vicinity of the X $^2\Pi_{3/2}$ v^+ = 0 ← X $^1\Sigma^+$ and the X $^2\Pi_{1/2}$ v^+ = 0 ← X $^1\Sigma^+$ photoionizing transitions in HBr. The spectrum was generated with a 10 meV window for the electron kinetic energy and corrected for the photon flux and pressure variations over the course of the scan. Also shown is an optimized simulation of the spectrum (red), corresponding to the stick spectrum broadened with a Gaussian function, (see text for details). The rotational temperature that resulted in the optimized simulation corresponded to 60 K ± 10 K. (b) The threshold photoelectron spectrum (blue) showing the band due to the X $^2\Pi_{3/2}$ v^+ = 0 ← X $^1\Sigma^+$ photoionizing transition, and the simulated spectrum (red). Also plotted is a stick spectrum (green) showing the contribution from each transition contributing to the simulated spectrum, (see text for details). The labels shown in (a) and (b) correspond to the cationic states involved in the transitions.

the $^2\Pi_{3/2}$ v^+ = 0 band. This band exhibits partially resolved rotational structure, while the $^2\Pi_{1/2}$ v^+ = 0 band does not. This observation is likely due to a combination of the lower J^+ levels accessed in the latter band, and the larger Λ-doubling constant in that band [34], both of which will increase spectral congestion. Fig. 4(b) shows a simulated stick spectrum of the X $^2\Pi_{3/2}$ v^+ = 0 ← X $^1\Sigma^+$ transition, and a convolution of the predicted structure with a 3.7 meV (FWHM) Gaussian envelope, corresponding approximately to the spectral resolution of the TPES. This simulation reproduces both the observed rotational structure in the $^2\Pi_{3/2}$ band and the band shape.

The simulation was performed by using a Boltzmann distribution for the initial rotational populations and varying the ionization energy and relative intensities of the $\Delta J = J^+ - J$ branches with ΔJ = ± 1/2, ± 3/2, ± 5/2, and ± 7/2. This range is consistent with the dominance of ionization processes with photoelectrons having $l \leq 2$. The spectroscopic constants for the ground states of HBr and HBr^+ have been well characterized in previous work [35,34], and they were used without modification in the present work. In obtaining the optimized simulated spectrum, the rotational temperature, the ionization energy, the relative intensities of the two spin–orbit bands, and the relative rotational branch intensities were all varied. Because the rotational structure was not resolved for the $^2\Pi_{1/2}$ band, the same branch intensities were used

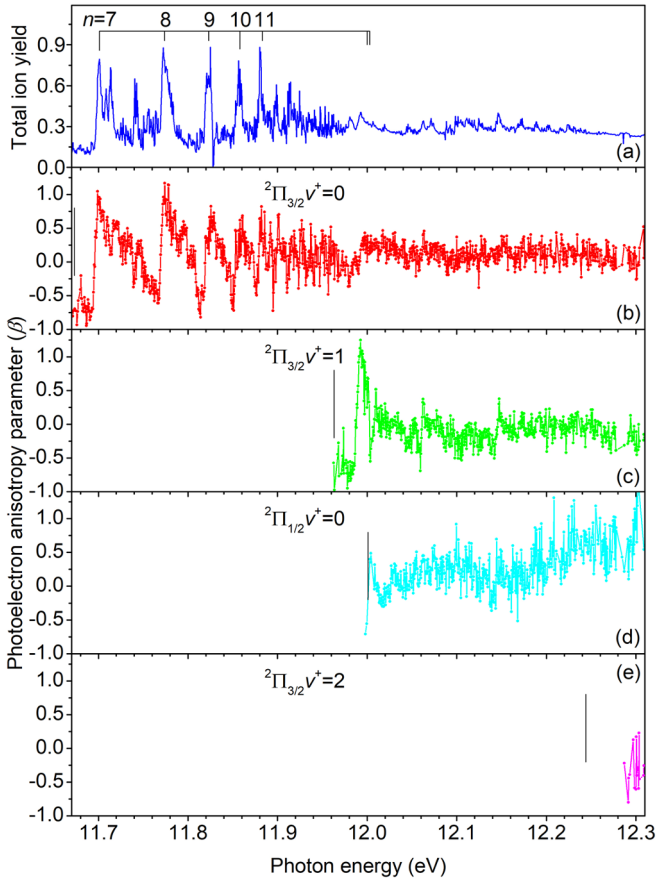

Fig. 5. The total ion yield (a), and the photoelectron anisotropy parameters (β) of the HBr^+ X $^2\Pi_{3/2}$ $v^+ = 0$ (b), $^2\Pi_{3/2}$ $v^+ = 1$ (c), $^2\Pi_{1/2}$ $v^+ = 0$ (d), and $^2\Pi_{3/2}$ $v^+ = 2$ (e) states. The vertical lines in panels (b) – (e) mark the measured vertical ionization energies [12]. The Rydberg series indicated in panel (a) corresponds to the $nd(J^+ = 5/2, j = 2.5)$ series assigned by Irrgang et al [15]. The calculated excitation energies [15] of the Rydberg states are marked. The two short, closely spaced, vertical lines in (a) indicate the calculated ionization energy [15].

for both components and optimized with the rotationally resolved $^2\Pi_{3/2}$ band. This leads to a very good agreement between the simulation and the experimental spectrum for the lower spin–orbit component band but to observable rotational-branch intensity disagreements for the upper one (see discussion below). The optimized simulation of the relative branch intensities for ΔJ = -7/2, −5/2, −3/2, −1/2, 1/2, 3/2, 5/2, and 7/2 was obtained with values of 0.2, 0.7, 1.0, 1.0, 0.8, 1.0, 0.5, and 0.2, respectively. In the high-resolution ZEKE spectrum of Irrgang et al. [17], the branch intensities appear to fall off more rapidly with increasing $|\Delta J|$. The larger $|\Delta J|$ values observed here could be a result of the broader electron energy window (electrons having kinetic energies up to 10 meV were included) used in producing the TPES, which might increase the contribution from autoionizing resonances. The time-delay used in the ZEKE measurements also minimizes the contributions from autoionizing resonances.

The ionization energies measured in the present work are red-shifted by the electric field. The TPES (which corresponds to transitions between neutral and cationic vibronic states), displayed as a function of photon energy, is shifted to lower energy compared to the field-free spectrum. The formula used to evaluate this shift due to the electric field is $\Delta E = 6\sqrt{F}$, where the units of ΔE are cm^{-1} and those of F are V/cm [36] When corrected for the electric field shift (5.0 meV in our work), the optimized simulated spectrum resulted in an ionization energy of 11.6673 ± 0.0010 eV, in excellent agreement with previous values [14,16,17]. The optimized spectrum was obtained with a rotational temperature of 60 K ± 10 K, in agreement with our estimated value from the translational temperature of the HBr beam (see Section 2).

The resonances due to autoionization appear at the energy of transitions into highly excited neutral states. These neutral states are split by the Stark effect (but not shifted). However, the splitting is not resolved and just appears as a broadening of the levels.

The simulation of the $^2\Pi_{1/2}$ band in Fig. 4(a) is not as good as that of the $^2\Pi_{3/2}$ band, which can be understood as follows. First, the simulated relative intensity of the $^2\Pi_{3/2}$ band to that of the $^2\Pi_{1/2}$ band is 1:0.54, as compared to the statistical ratio of 1:1. This observation strongly suggests that autoionization is affecting the intensity of the $^2\Pi_{3/2}$ band, as is consistent with the rotational branch intensities. Indeed, Irrgang et al. have previously noted intensity perturbations in their ZEKE spectrum [17]. Second, as indicated above, this effect appears to enhance the intensity of the branches with larger ΔJ in the $^2\Pi_{3/2}$ band. If this effect is less important or absent in the upper spin–orbit component, the use of the $^2\Pi_{3/2}$ branch intensities artificially shifts the band maximum and produces a simulated band that is broader than the experimental spectrum, as observed in Fig. 4(a). Unfortunately, without resolving the rotational structure in the $^2\Pi_{1/2}$ band, this interpretation cannot be confirmed.

3.2. Photoelectron angular distributions

Fig. 5 shows the total ion yield and the photoelectron anisotropy parameters associated with the $^2\Pi_{3/2}$ $v^+ = 0$, 1, 2 and the $^2\Pi_{1/2}$ $v^+ = 0$ states over the photon energy range 11.67–12.31 eV, and Fig. 6 displays the total ion yield and the β-parameter for the $^2\Pi_{3/2}$ $v^+ = 0$ state over a more limited excitation range. In general, the energy dependent variations in the two sets of results for the β-parameter associated with the $^2\Pi_{3/2}$ $v^+ = 0$ state are in good agreement.

Most of the structure in the ion yield in the energy range 11.69 – 12.00 eV (Fig. 5(a) and 6(a)) can be attributed to *n*s, *n*p, *n*d and *n*f Rydberg series converging onto the $^2\Pi_{1/2}$ $v^+ = 0$ threshold. The assignments of these Rydberg series have been discussed extensively [13–15]. The Rydberg states of low principal quantum number ($n = 5 - 9$) were investigated theoretically by Lefebvre-Brion et al. [13] using multichannel quantum defect theory and Hund's coupling case (a) [37]. The results from those calculations provided a satisfactory interpretation for some of the prominent peaks observed in the ion yield just above threshold. Moreover, the inclusion of vibrationally excited levels was shown to be important. Irrgang et al. [14] found that for $n \leq 11$, an interpretation of the structure appearing in the jet-cooled photoelectron yield using a description of the angular momentum coupling according to Hund's case (c) [37] was appropriate, while for higher Rydberg members, Hund's case (e) [37] seemed more suitable. The interpretation proposed by Irrgang et al. [14], based upon quantum defect considerations, allowed most of the structure to be assigned. A subsequent reinvestigation [15], where the Rydberg states converging onto the X $^2\Pi_{1/2}$ thresholds were represented in a coupling case intermediate between Hund's case (a) and case (e) indicated that some of the assignments required modification.

For simplicity, only one Rydberg series has been marked in Fig. 5(a) and 6(a). This series has been assigned as $nd\delta$ $J^+ = 1/2$, where J^+ denotes the total angular momentum of the molecular ion, by Irrgang et al. [14], and as *n*d $J^+ = 5/2$, $j = 2.5$, where J^+ denotes the rotational angular momentum of the ion core and j denotes the total angular momentum of the photoelectron, by Irrgang et al. [15]. The images shown in Fig. 1(a) and 1(b) demonstrate the effect of autoionization on the $^2\Pi_{3/2}$ $v^+ = 0$ state photoelectron angular distributions. At a photon energy of 11.766 eV (Fig. 1(a)), where ionization arises mainly from direct processes, the β-parameter is negative, and electron ejection occurs predominantly in a direction perpendicular to the polarization axis. In contrast, at a photon energy of 11.774 eV (Fig. 1(b)), coinciding with transitions into the 8d Rydberg state (Fig. 5(a)), autoionization

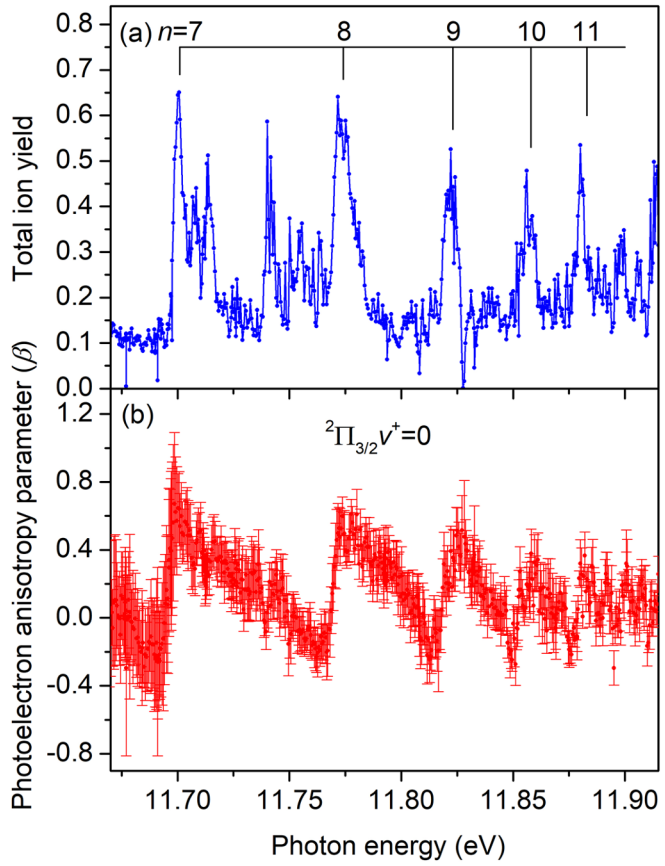

Fig. 6. (a) The total ion yield and (b) the photoelectron anisotropy parameter of the HBr^+ X $^2\Pi_{3/2}$ $v^+ = 0$ state. The average value of the β-parameter, and the uncertainty, have been estimated according to Eqs (2) and (3). The Rydberg series indicated in panel (a) corresponds to the $nd(J^+ = 5/2, j = 2.5)$ series assigned by Irrgang et al [15]. The calculated excitation energies [15] of the Rydberg states are marked in (a).

leads to a positive β-parameter, with electrons being ejected predominantly in a direction parallel to the polarization axis.

The profiles of the peaks in the prominent nd series in HBr (Fig. 5(a)) display asymmetric Fano profiles [38] similar to those of the $4p^6(^1S_0) \rightarrow 4p^5(^2P_{1/2})nd$ transitions in krypton [4–6,26]. In particular, the corresponding resonance profiles in HBr show a steep rise and more gradual fall with increasing energy. Such asymmetric profiles arise from the interference between direct and indirect ionization processes. As a result, the partial wave composition of the outgoing electron also varies substantially across the resonance. Because the photoelectron angular distributions reflect the interference among the outgoing partial waves, the β-parameter is thus expected to vary across the peaks, as is observed in Fig. 5(b) and 6(b). The variation of β across the nd resonances in HBr is similar to what is observed in krypton.

In the region of the spectrum lying between the $^2P_{3/2}$ and the $^2P_{1/2}$ spin–orbit split ionization thresholds of rare gases like krypton and xenon, β is determined by the relative contributions of parity-favoured and parity-unfavoured processes involving photoelectrons with $l = 2$ and parity-favoured processes involving photoelectrons with $l = 0$ [3]. The parity unfavoured $l = 2$ process has $\beta = -1$, while the parity-favoured $l = 0$ and 2 processes have $\beta = 0$ and 1, respectively [3]. At the minima of the nd resonances in Kr, the parity-unfavoured $l = 2$ continuum and parity-favoured $l = 0$ continuum dominate, leading to a negative value of β, while near the maximum of the resonances, the parity-favoured $l = 2$ process dominates, leading to β near 1. The β-value shows a similar asymmetric lineshape across the very sharp, intense ns resonances, approaching 0 near the ns resonance maxima where the parity-favoured $l = 0$ continuum dominates.

Although there are more ionization continua in HBr, leading to more complicated behaviour that tends to wash out the resonance structure in the β-value, the overall β curve is quite similar to that in Kr. In particular, the β curve shows the same asymmetry in the resonance profiles as the broad nd series, suggesting a similar variation in the relative importance of the parity favoured and unfavoured continua with $l = 2$. Such behaviour was also observed by Carlson et al. [39] for the β-parameter associated with the HI^+ X $^2\Pi_{3/2}$ $v^+ = 0$ level in the region between the $^2\Pi_{3/2}$ and $^2\Pi_{1/2}$ ionization thresholds. The features in the β curve corresponding to the sharper resonances converging to the HBr^+ $^2\Pi_{1/2}$, $v^+ = 0$ threshold are weak, but smaller excursions in the β-values are clearly visible.

Above the $^2\Pi_{3/2}$ $v^+ = 1$ ionization threshold at 11.963 eV [12], the structure in the ion yield becomes weaker (Fig. 5(a)), and the average value of the β-parameter for the $^2\Pi_{3/2}$ $v^+ = 0$ level, over the 12.0 – 12.3 eV excitation range, remains slightly positive (Fig. 5(b)). The β-parameters for the $^2\Pi_{3/2}$ $v^+ = 1$ (Fig. 5(c)) and the $^2\Pi_{1/2}$ $v^+ = 0$ (Fig. 5(d)) states are generally close to zero, indicating a fairly isotropic electron angular distribution, although that for the $^2\Pi_{1/2}$ $v^+ = 0$ state becomes positive as the excitation energy increases.

Fig. 7 shows the experimental results in greater detail over the photon energy range 11.68 – 11.76 eV, together with the theoretically predicted β-parameter [15] and assignments of the Rydberg states [15]. In the energy range 11.709 – 11.716 eV, three peaks were observed in the electron yield measured by Irrgang et al. [14], and assigned to the 7s ($J^+ = 1/2$,), 7d ($J^+ = 7/2$) and 7s ($J^+ = 3/2$) Rydberg states in order of increasing energy (see Irrgang et al. [15] for details regarding these assignments). The third of these peaks, at the highest excitation

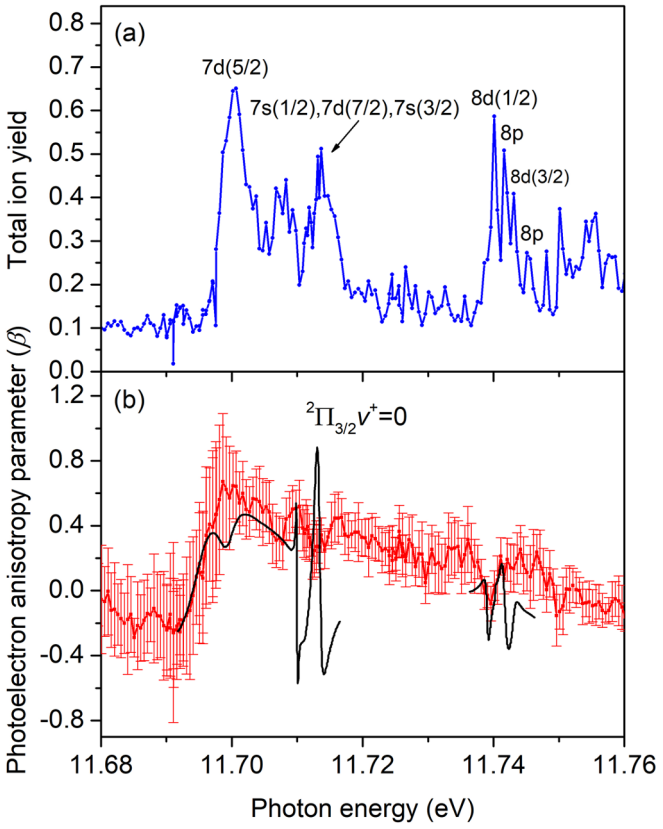

Fig. 7. (a) The total ion yield and (b) the photoelectron anisotropy parameter of the HBr^+ X $^2\Pi_{3/2}$ $v^+ = 0$ state. The average value of the β-parameter (red), and the uncertainty, have been estimated according to Eqs (2) and (3). The assignments for the Rydberg states shown in panel (a) have been taken from Irrgang et al [15]. The calculated β-parameter (black) plotted in panel (b) has been taken from Irrgang et al [15].

energy, is a doublet [14], with the second contribution probably arising from the 5d $J^+ = 7/2$ level of the $^2\Pi_{1/2}$ $v^+ = 1$ core [15]. The calculated β-parameter displays significant variations (Fig. 7(b)), especially in the vicinity of these Rydberg states. The combination of rotational structure and finite wavelength resolution tends to smear out the resonances in the β-parameters predicted by the theory. Nevertheless, our measured β-parameter exhibits a distinct local minimum at an excitation energy of 11.712 eV that appears to correlate with these autoionizing resonances. Another local minimum is observed in the experimental data at 11.708 eV, and this seems to correlate with an unassigned peak appearing in both the present ion yield and the previous electron yield [14]. The two broad maxima in the calculated β-parameter in the region of the 7d ($J^+ = 5/2$) Rydberg state around 11.701 eV are in reasonable accord with the experimental results. Although the variations in the $^2\Pi_{3/2}$ $v^+ = 0$ state β-parameter are fairly small, they are present in the measurements obtained in both sets of our experimental data.

In the second energy range (11.736–11.746 eV) studied theoretically by Irrgang et al. [15], the structure observed in the electron yield [14] was attributed to four Rydberg states. These states, assigned as 8d ($J^+ = 1/2$), 8p, 8d ($J^+ = 3/2$) and 8p, are marked in Fig. 7(a), and the calculated β-parameter is also plotted (Fig. 7(b)). Our experimental β-values exhibit a local minimum at a photon energy of 11.739 eV, which approximately coincides with the 8d ($J^+ = 1/2$) state, but our results show no evidence of the second predicted minimum around 11.742 eV.

Mank et al. [40] have measured the β-parameter for the HI^+ X $^2\Pi_{3/2}$ $v^+ = 0$ state in the photon energy range 10.717–10.787 eV. This energy range lies between the $^2\Pi_{3/2}$ and $^2\Pi_{1/2}$ ionization thresholds and contains several Rydberg states belonging to series converging onto the $^2\Pi_{1/2}$ state limit. A comparison between the experimental [40] and theoretical [41] β-parameters showed that whereas the predicted autoionization from the pπ, dπ and dδ Rydberg states affects the measured angular distributions, little evidence is observed of the rapid variations predicted in the vicinity of the very narrow resonances associated with the fσ, fπ or sσ states.

4. Summary

The HBr^+ X $^2\Pi_{3/2}$ $v^+ = 0$, 1, 2 and the $^2\Pi_{1/2}$ $v^+ = 0$ state photoelectron anisotropy parameters, and the total ion yield, have been measured with a double-imaging photoelectron-photoion spectrometer and synchrotron radiation in the photon energy range 11.67 – 12.31 eV. In particular, a detailed study has been made of the $^2\Pi_{3/2}$ $v^+ = 0$ state photoelectron anisotropy parameter in the region encompassing the Rydberg states belonging to series converging onto the $^2\Pi_{1/2}$ ionization limit. These states, which have been identified using the assignments from previously reported calculations [15], give rise to prominent structure in the ion yield.

The $^2\Pi_{3/2}$ $v^+ = 0$ β-parameter determined in the present experiment has been compared to earlier theoretical predictions [15], and discussed in relation to those for the Kr^+ $4p^5$ $^2P_{3/2}$ state [4–6,26]. Autoionization from the Rydberg states belonging to one of the d-type series converging onto the $^2\Pi_{1/2}$ $v^+ = 0$ ionization limit produces significant variations in the $^2\Pi_{3/2}$ $v^+ = 0$ anisotropy parameter. These variations exhibit an energy dependence similar to that observed in the β-parameter associated with the Kr^+ $4p^5$ $^2P_{3/2}$ ionic state in the energy range encompassing the autoionizing resonances due to the $4p^6(^1S_0) \rightarrow 4p^5(^2P_{1/2})nd$ transitions.

Dill [3] has discussed the energy dependence of the β-parameter, in the region of the spectrum lying between the ground $^2P_{3/2}$ and excited $^2P_{1/2}$ spin–orbit split ionization thresholds of the heavier rare gases, in terms of parity-favoured and parity-unfavoured processes. For a particular partial wave representing the outgoing electron, these parity-favoured and parity-unfavoured processes have specific β-values. The relative contributions of such processes provide a satisfactory description of the energy dependent variations in β in the vicinity of autoionizing resonances. It appears that the observed energy dependence of the $^2\Pi_{3/2}$ $v^+ = 0$ photoelectron anisotropy parameter in HBr, in regions affected by autoionization, may be interpreted in a similar manner.

Theoretical predictions for the $^2\Pi_{3/2}$ $v^+ = 0$ β-parameter, and also for the electron spin polarization parameter A, have been provided by Irrgang et al. [15] over selected photon energy ranges. A comparison between the present experimental and calculated [15] β-values shows some similarities, especially in energy regions encompassing broad autoionizing resonances, but little evidence has been found for the rapid variations predicted to occur over narrow energy ranges associated with some of the other autoionizing resonances. This discrepancy may, in part, be attributed to a lack of sufficient resolution in the experimental measurements. However, discrepancies were also evident in the comparison between the measured and calculated spin polarization parameters [15]. An improved understanding of the photoionization dynamics requires further experimental measurements, in particular ones in which the final ionic states are rotationally resolved, as well as more comprehensive theoretical studies.

CRediT authorship contribution statement

H.R. Hrodmarsson: Data curation, Investigation. **B. Gans:** Data curation, Formal analysis. **S. Boyé-Péronne:** Data curation, Investigation. **G.A. Garcia:** Methodology, Formal analysis. **L. Nahon:** Project administration. **S.T. Pratt:** Investigation, Writing - review & editing. **D.M.P. Holland:** Investigation, Writing - review & editing.

Declaration of Competing Interest

The authors declare that they have no known competing financial interests or personal relationships that could have appeared to influence the work reported in this paper.

Acknowledgements

DMPH is grateful to the Science and Technology Facilities Council (United Kingdom) for financial support. STP is supported by the U.S. Department of Energy, Office of Science, Office of Basic Energy Sciences, Division of Chemical Sciences, Geosciences, and Biosciences under contract No. DE-AC02-06CH11357. We are grateful to Oksana Travnikova (Sorbonne Université, Paris) for the loan of a cylinder of hydrogen bromide. We acknowledge the provision of beamtime by Synchrotron SOLEIL (beamtime Proposal No. 20170891), and we thank the technical staff at SOLEIL for their support and for the smooth operation of the facility.

References

[1] V.L. Sukhorukov, I.D. Petrov, M. Schäfer, F. Merkt, M.-W. Ruf, H. Hotop, J. Phys. B 45 (2012) 092001.
[2] J. Berkowitz, Photoabsorption, Photoionization, and Photoelectron Spectroscopy, Academic Press, New York, 1979.
[3] D. Dill, Phys. Rev. A 7 (1973) 1976.
[4] Y. Morioka, M. Watanabe, T. Akahori, A. Yagishita, M. Nakamura, J. Phys. B 18 (1985) 71.
[5] J.Z. Wu, S.B. Whitfield, C.D. Caldwell, M.O. Krause, P. van der Meulen, A. Fahlman, Phys. Rev. A 42 (1990) 1350.
[6] D.R. Cooper, D. Cubric, D.B. Thompson, P. Bolognesi, M.C.A. Lopes, G.C. King, J. Electron Spectrosc. Relat. Phenom. 112 (2000) 129.
[7] H.J. Lempka, T.R. Passmore, W.C. Price, Proc. Roy. Soc. Lond. A 304 (1968) 53.
[8] D.W. Turner, C. Baker, A.D. Baker, C.R. Brundle, Molecular Photoelectron Spectroscopy, Wiley-Interscience, London, 1970.
[9] J. Delwiche, P. Natalis, J. Momigny, J. E. Collin, J. Electron Spectrosc. Relat. Phenom. 1 (1972/73) 219.
[10] K. Kimura, S. Katsumata, Y. Achiba, T. Yamazaki, S. Iwata, Handbook of HeI Photoelectron Spectra of Fundamental Organic Molecules, Japan Scientific Societies Press, Tokyo, 1981.
[11] A.J. Yencha, M.-W. Ruf, H. Hotop, Z. Phys. D 21 (1991) 113.
[12] A.J. Yencha, A.J. Cormack, R.J. Donovan, K.P. Lawley, A. Hopkirk, G.C. King,

Chem. Phys. 238 (1998) 133.
[13] H. Lefebvre-Brion, P.M. Dehmer, W.A. Chupka, J. Chem. Phys. 85 (1986) 45.
[14] R. Irrgang, N. Böwering, M. Drescher, M. Spieweck, U. Heinzmann, J. Chem. Phys. 104 (1996) 8966.
[15] R. Irrgang, M. Drescher, M. Spieweck, U. Heinzmann, N.A. Cherepkov, H. Lefebvre-Brion, J. Chem. Phys. 108 (1998) 10070.
[16] N.P.L. Wales, W.J. Buma, C.A. de Lange, H. Lefebvre-Brion, K. Wang, V. McKoy, J. Chem. Phys. 104 (1996) 4911.
[17] R. Irrgang, M. Drescher, F. Gierschner, M. Spieweck, U. Heinzmann, J. Electron Spectrosc. Relat. Phenom. 80 (1996) 5.
[18] T.A. Carlson, A. Fahlman, M.O. Krause, T.A. Whitley, F.A. Grimm, J. Chem. Phys. 81 (1984) 5389.
[19] H. Lefebvre-Brion, M. Salzmann, H.-W. Klausing, M. Müller, N. Böwering, U. Heinzmann, J. Phys. B 22 (1989) 3891.
[20] M. Salzmann, N. Böwering, H.-W. Klausing, R. Kuntze, U. Heinzmann, J. Phys. B 27 (1994) 1981.
[21] M. Salzmann, N. Böwering, H.-W. Klausing, U. Heinzmann, Z. Phys, D 36 (1996) 137.
[22] G. Raseev, F. Keller, H. Lefebvre-Brion, Phys. Rev. A 36 (1987) 4759.
[23] G.A. Garcia, B.K. Cunha de Miranda, M. Tia, S. Daly, L. Nahon, Rev. Sci. Instrum. 84 (2013) 053112.
[24] X. Tang, G.A. Garcia, J.-F. Gil, L. Nahon, Rev. Sci. Instrum. 86 (2015) 123108.
[25] L. Nahon, N. de Oliveira, G.A. Garcia, J.-F. Gil, B. Pilette, O. Marcouillé, B. Lagarde, F. Polack, J. Synchrotron Radiat. 19 (2012) 508.
[26] W.R. Johnson, K.T. Cheng, K.-N. Huang, M. Le Dourneuf, Phys. Rev. A 22 (1980) 989.
[27] B. Mercier, M. Compin, C. Prevost, G. Beller, R. Thissen, O. Dutuit, L. Nahon, J. Vac. Sci. Technol. A 18 (2000) 2533.
[28] A.T.J.B. Eppink, D.H. Parker, Rev. Sci. Instrum. 68 (1997) 3477.
[29] D.M.P. Holland, E.A. Seddon, S. Daly, C. Alcaraz, C. Romanzin, L. Nahon, G.A. Garcia, J. Phys. B 46 (2013) 095102.
[30] G.A. Garcia, L. Nahon, I. Powis, Rev. Sci. Instrum. 75 (2004) 4989.
[31] J. Cooper, R.N. Zare, J. Chem. Phys. 48 (1968) 942.
[32] G.A. Garcia, H. Soldi-Lose, L. Nahon, Rev. Sci. Instrum. 80 (2009) 023102.
[33] L. Minnhagen, J. Opt. Soc. Am. 63 (1973) 1185.
[34] K.G. Lubic, D. Ray, D.C. Hovde, L. Veseth, R.J. Saykally, J. Mol. Spectrosc. 134 (1989) 21.
[35] K. P. Huber, G. Herzberg, Molecular Spectra and Molecular Structure, vol. IV. Constants of Diatomic Molecules, Van Nostrand Reinhold, New York, 1979.
[36] T.F. Gallagher, Rydberg Atoms, Cambridge University Press, Cambridge, 1994.
[37] H. Lefebvre-Brion, R.W. Field, The Spectra and Dynamics of Diatomic Molecules, Elsevier, Amsterdam, 2004.
[38] U. Fano, Phys. Rev. 124 (1961) 1866.
[39] T.A. Carlson, P. Gerard, M.O. Krause, G. Von Wald, J.W. Taylor, F.A. Grimm, J. Chem. Phys. 84 (1986) 4755.
[40] A. Mank, M. Drescher, T. Huth-Fehre, G. Schönhense, N. Böwering, U. Heinzmann, J. Phys. B 22 (1989) L487.
[41] H. Lefebvre-Brion, A. Giusti-Suzor, G. Raseev, J. Chem. Phys. 83 (1985) 1557.